



Effect of adding organo-modified montmorillonite nanoclay on the performance of oil-well cement paste in CO₂-rich environments

Martimiano K. Moraes, Eleani Maria da Costa ^{*}

School of Technology, Pontifical Catholic University of Rio Grande do Sul, 6681 Ipiranga Avenue, Building 30, Room 111/F, 90619-900, Porto Alegre, RS, Brazil

ARTICLE INFO

Keywords:

Nanoparticles
Nanoclay
Oil-well cement
CO₂-Environment

ABSTRACT

This work studies the influence of incorporating organo-modified montmorillonite (OMMT) nanoclay in class G cement pastes on chemical and mechanical resistance in CO₂-rich environments. Cement paste specimens, with and without added nanoclay (0.5%, 1%, 2% in wt.), were submitted to degradation tests in CO₂-saturated water and wet supercritical CO₂, at 90 °C and 15 MPa. Scanning electron microscopy, X-ray diffraction, computed X-ray microtomography, pycnometry, Vickers microhardness measurements, and compressive strength tests were used to evaluate the effect of the OMMT nanoclay on the cement paste properties. The addition of 0.5% OMMT nanoclay increased the specific density and the compressive strength of hardened cement paste and decreased chemically modified layer as a result of CO₂ attack. However, these effects became less evident with increasing OMMT nanoclay content. Additionally, the Vickers microhardness and compressive strength results suggest that OMMT nanoclay can prevent the high precipitation of carbonates that influences the diffusion of CO₂ into cement paste.

1. Introduction

Carbon capture and storage (CCS) in geological formations shows much promise as a technology for mitigating CO₂ emissions, the main greenhouse gas [1–8]. CCS consists of capturing and separating the CO₂ released from a stationary source, and then transporting it to storage sites for injection into geological formations. Examples of such sites include oil- and gas-depleted fields, saline aquifers, and deep coal beds [2–4,9–11]. The CO₂ is injected in the supercritical state (the critical point corresponds to 7.38 MPa and 31 °C) to allow the storage of large amounts of CO₂, at depths recommended to exceed 800 m [3,12]. CO₂ solubility in water decreases with increasing salinity and temperature and improves with increasing pressure. Although CO₂ has been injected into geological formations for several decades for various purposes, including enhanced oil recovery (EOR), long-term CO₂ storage is a relatively new concept. The use of this technology requires the maintenance of the integrity of the injection wells over time in order to prevent CO₂ leakage [13]. Cement paste is used to insulate the wells by filling the cylindrical gap between the steel casing and the drilled rock. Therefore, the cement paste must ensure the structural integrity of the well and geological formations during hydrocarbon exploration and CO₂ injection and storage over long time periods. In addition, cement paste

can also be used to form a sealing plug over an abandoned well. Many studies have shown that the cement paste typically used in wells can undergo chemical changes in CO₂-rich environments resulting from carbonic acid attack, which affects its properties and compromises well integrity [14–21]. Chemical reactions of cement paste in CO₂ medium are shown in Table 1. The CO₂ dissolved in the formation fluids reacts with the hydrate products of the cement paste, calcium hydroxide (Ca(OH)₂-portlandite), and calcium silicate hydrate (CSH) to form calcium carbonate (CaCO₃). From a consideration of the thermodynamic free energy, the portlandite is consumed first, producing a highly porous zone (portlandite-depleted zone). The precipitation of calcium carbonate (CaCO₃) in the cement pores produces a zone of low porosity and high hardness (carbonated zone). However, as Ca(OH)₂ is consumed, the pH of the pore solution decreases and the dissolution of the previously precipitated calcium carbonate begins, creating a highly porous zone (bicarbonation zone). Once the portlandite is consumed, the CSH is attacked, forming amorphous silica gel [5,17–19].

Alternative solutions designed to prevent or minimize the degradation of cement paste under carbon geological storage conditions have been tested [14,15,22]. The use of pozzolanic materials has attracted particular interest since it decreases permeability and reduces amount of portlandite that forms CSH as secondary product, hindering CO₂

^{*} Corresponding author.

E-mail address: eleani@pucrs.br (E. Maria da Costa).

<https://doi.org/10.1016/j.cemconcomp.2021.104400>

Received 18 February 2020; Received in revised form 4 June 2021; Accepted 27 December 2021

Available online 4 January 2022

0958-9465/© 2022 Elsevier Ltd. All rights reserved.

Table 1Chemical reactions involved in the cement degradation process in the presence of CO₂.

CO ₂ Dissociation	
Reaction 1	$\text{CO}_2 + \text{H}_2\text{O} \leftrightarrow \text{H}_2\text{CO}_3 \leftrightarrow \text{H}^+ + \text{HCO}_3^- \leftrightarrow 2\text{H}^+ + \text{CO}_3^{2-}$
Cement Paste Carbonation	
Reaction 2	$\text{Ca(OH)}_{2(s)} + 2\text{H}^+ + \text{CO}_3^{2-} \rightarrow \text{CaCO}_{3(s)} + 2\text{H}_2\text{O}$
Reaction 3	$\text{C}_{3,4}\text{-S}_2\text{-H}_{8(s)} + 2\text{H}^+ + \text{CO}_3^{2-} \rightarrow \text{CaCO}_{3(s)} + \text{SiO}_x\text{OH}_x (s)$
Reaction 4	$\text{Ca(OH)}_{2(s)} + \text{H}^+ + \text{HCO}_3^- \rightarrow \text{CaCO}_{3(s)} + 2\text{H}_2\text{O}$
Reaction 5	$\text{C}_{3,4}\text{-S}_2\text{-H}_{8(s)} + \text{H}^+ + \text{HCO}_3^- \rightarrow \text{CaCO}_{3(s)} + \text{SiO}_x\text{OH}_x (s)$
Bicarbonation	
Reaction 6	$\text{CO}_2 + \text{H}_2\text{O} + \text{CaCO}_{3(s)} \leftrightarrow \text{Ca}^{2+} + 2\text{HCO}_3^-$
Reaction 7	$2\text{H}^+ + \text{CaCO}_{3(s)} \leftrightarrow \text{CO}_2 + \text{Ca}^{2+} + \text{H}_2\text{O}$

diffusion and consequently minimizing cement carbonation [23–27]. On the other hand, advances in nanotechnology have contributed to the improvement of cement-based material performance. The use of nanoparticles in cement pastes has generated much interest since they have the potential to provide new material functionalities and because some nanoparticles can enhance properties such as high strength, low permeability and porosity, enhanced durability, low retraction, cracking self-control, and good adhesion to steel [28–30]. Silica (SiO₂), alumina (Al₂O₃), titanium dioxide (TiO₂), zinc dioxide (ZnO₂), and calcium carbonate (CaCO₃) are examples of nanoparticles that have been added to cement-based material [14,31–37]. Nanoparticles, such as silica (SiO₂) and alumina (Al₂O₃), affect the mechanical properties of cement pastes strongly because of their high chemical reactivity, which stems from their large surface area, and by acting as a filler in the interstices between the cement grains, resulting in a denser matrix. Furthermore, these nanoparticles act as nucleation sites, accelerating the hydration process. Because of their high reactivity, they accelerate pozzolanic reactions, producing additional amounts of CSH gel and forming smaller Ca(OH)₂ and CSH crystals [29,31,33]. Among the various nanoparticle types, lamellar nanoparticles such as clays are of special interest, given their high aspect ratio, pozzolanic nature and relatively low cost. They may also carry a surface charge capable of interacting with other material structures [38–41]. Kuo et al. [38] showed that adding hydrophobic organo-modified montmorillonite (OMMT) micro-particles to cement mortars improves their strength and can produce a diffusion barrier around capillary pores. Additionally, Yu et al. [41] observed that the damping properties of cement paste are improved by the presence of OMMT.

However, studies involving the addition of nanoparticles to cement pastes used for oil-wells are scarce in the literature. The main challenge is to achieve an adequate dispersion of the nanoparticles. The formation of particle agglomeration affects the rheological behavior of slurry and the properties of the cement paste. Given the difficulty of dispersing particles during mixing, some authors suggest an appropriate percentage of nanoparticle of approximately 1%–5% by weight of cement [14, 33]. Since the addition of some nanoparticles can reduce the cement paste permeability and porosity, in principle they could also decrease the diffusion of acid solution into the matrix and enhance properties such as the mechanical strength and the durability of the cement paste when exposed to a CO₂-rich environment. Thus, the present work investigates the effect of incorporating OMMT nanoclay on the degradation of class G cement paste (employed for the completion and abandonment of oil-wells) in media containing CO₂ at a high pressure and high temperature (HPHT).

2. Materials and methods

2.1. Organo-modified montmorillonites (OMMT) preparation

Clays are either expandable or non-expandable. Well-known examples of expandable clays are smectites. These include montmorillonite (MT), whose chemical structure consists of an edge-shared octahedral

sheet with aluminum or magnesium hydroxide and two silicate tetrahedral layers with sodium or calcium cations [38]. Typically, MT particles are highly hydrophilic and the water absorbed in the region between the layers causes their expansion, which can drastically affect the cement slurry workability and induce microcracks in the cementitious matrix because water is absorbed in the interlayer regions between silicate layers. One way to overcome this problem is through cation exchange. By replacing sodium or calcium in the interlamellar layer with organic cations, hydrophilicity is reduced, and the material becomes organophilic and at the same time the organic cations increase the interplanar distance between layers promoting the clay expansion prior its addition to cement [30,42]. When properly exfoliated, the silicate layer thicknesses are of the order of 1 nm and can thus be utilized to improve the microstructure and mechanical properties of cement pastes and impede the diffusion of aggressive agents [30,38,41,42].

In this work, MT was obtained from natural sodium bentonite (aluminum phyllosilicate clay) supplied by Schumacher Insumos (Brazil), and the organo-modified montmorillonites (nanoclay) were achieved by cation exchange of interlayer cations with quaternary ammonium cations (hexadecyltrimethyl ammonium bromide) according to procedure described below. This cationic surfactant increases the interplanar distance between layers promoting the clay expansion prior adding to cement [38,40–42]. To separate the clay fraction from bentonite, ultrasonic centrifugation was used to disperse the particles for 5 min. Sieves with mesh numbers 200, 400, and 635 (openings size of 75 μm, 38 μm and 20 μm, respectively) were used successively to obtain particles smaller than the 20 μm. An X-ray pattern of smectite clay is shown in Fig. 1, displaying the high intensity characteristic peak associated with montmorillonite at 7.2° for the (001) crystallographic planes.

Before performing the Na cations substitution, a cation exchange capacity test was carried out by methylene blue adsorption according to the ASTM C 837-84 standard, yielding a MT cation exchange capacity of 90 meq/100 g. The replacement of Na cations was performed using a quaternary ammonium salt (hexadecyltrimethyl ammonium bromide) by dissolving 24 g of smectite in 1200 mL deionized water at 80 °C with mechanical stirring. A quaternary ammonium salt solution (7.9 g dissolved in 23.7 mL deionized water) was then added to the smectite solution, while continuing to stir for an additional 30 min. The solution was left to rest for 24 h and was then filtered using grade 3 qualitative filter paper and finally washed with 4 L of water to remove the remaining quaternary ammonium salt. The resulting material was dried

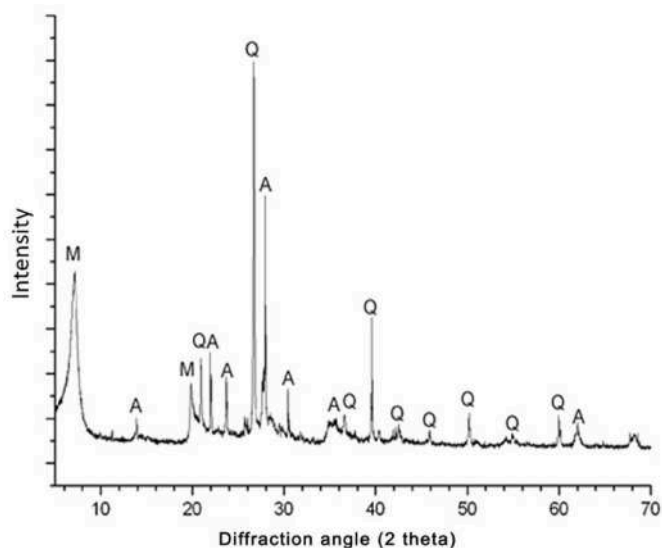


Fig. 1. X-ray pattern of natural sodium bentonite. A = albite; M = montmorillonite; Q = quartz.

for 24 h at 60 °C and then ground. Sieves were used to obtain particles smaller than a 635 mesh. Fig. 2a illustrates the microstructure of OMMT nanoclay, evidencing the presence of multilayers. X-ray diffraction analyses were performed to confirm the efficiency of the cation exchange process used for obtaining the OMMT. Fig. 2b shows the diffractogram of the OMMT nanoclay. In the X-ray spectrum, the main montmorillonite characteristic peak for (001) planes is shifted to a smaller angle, from 7.2° to approximately 4.5°. Bragg's law implies that the interlamellar distance for (001) planes increased from 12.3 Å to 19.6 Å, consistent with the replacement of sodium with quaternary ammonium salt.

2.2. Preparation of cementitious pastes and curing conditions

The cementitious pastes (without additives) were prepared according to the procedure established in the American Petroleum Institute (specification API 10A, 2009 [43]) using a 0.44 water/solid ratio. The standard cement paste (0% OMMT) was produced by stirring the water with oil-well class G cement for 15 s with a rotation speed of 4000 rpm, followed by 35 s at 12,000 rpm to complete the mixing. The amounts of OMMT nanoclay used were 0.5%, 1%, and 2% in weight replacing the cement. Due to hydrophobicity of OMMT particles, they are difficult to mix at the same time with water and cement. Therefore, the OMMT particles should be stirred vigorously in water to form a well-dispersed suspension solution before cement grains were added [38,40,42]. For cement pastes preparation, the OMMT particles were added slowly to water under continuous mechanical stirring at a speed of 1000 rpm during 3 h. After that, the cement was then added, and the mixing was performed as described above. The mini-slump test was used to evaluate the workability related to the yield stress of fresh cementitious pastes. It was performed using the Kantro method [44] by measuring the diameter of a pat (spread) formed by cement paste upon lifting of a mini-slump cone and the test results are expressed as an average over six measurements. The fresh cementitious pastes were poured into the cylindrical polymeric molds, producing specimens with a height of 46 mm and a diameter of 23 mm. The cement specimens were cured at 60 °C for 8 h prior to CO₂ degradation tests in a pressure vessel filled with distilled water by pressurizing nitrogen (N₂) until reach 6 MPa. These curing conditions produce more than 70% of reaction products for oil-well cement slurry and further hydration of cement is very slow [45]. After curing, the samples were immediately placed in the reactor for the degradation test in CO₂-rich media.

Pycnometry was used to determine the specific mass of the cementitious systems, and the analyses were performed with the Quantachrome Instruments multipycnometer, model MVP- 6DC, using nitrogen gas. For pycnometry analysis, the cured cement specimens were transversally cut at the middle producing cylindrical samples of 23 × 23mm.

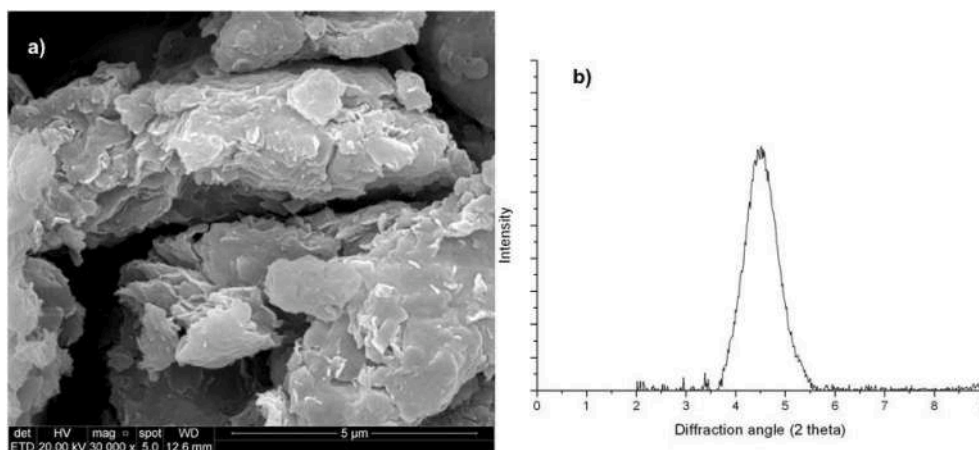


Fig. 2. (a) SEM image of organo-modified montmorillonite (OMMT) nanoclay. (b) X-ray diffraction from the (001) planes of organo-modified montmorillonite (OMMT).

The samples were oven-dried at 80 °C for 48 h prior to measurements. The heating until reach the set temperature was gradual to avoid cracking.

2.3. Degradation tests in a CO₂ environment at HPHT

Degradation tests were performed under a pressure of 15 MPa to simulate an oil-well of approximate depth 1.5 km, considering that the well pressure varies with a gradient of approximately 10 MPa km⁻¹ [46]. The temperature used in the experiments was 90 °C. Under these experimental conditions of temperature and pressure, the CO₂ is in the supercritical state, which is considered suitable for the geological storage of carbon. It is important to note that under geological reservoir conditions H₂O and CO₂ are two immiscible fluids, which means that CO₂ will stay on top (closest to the surface) due to the difference in density between CO₂ and H₂O. However, in contact interface between these two fluids occurs the dissolution of CO₂ into H₂O, and also H₂O in CO₂. Therefore, usually two phases coexist, wet supercritical CO₂ and aqueous solution saturated with CO₂ [1–4]. Thus, the experimental arrangement was designed to simultaneously obtains data representative of these two media: CO₂-saturated water-HSC (lower part of the reactor) and wet supercritical CO₂-WSC (upper part of the reactor), as illustrated in Fig. 3. For that, the cured cement specimens were distributed within a stainless-steel pressure vessel on two different levels with five specimens distributed at each level. Then, half of the reactor volume was filled with deionized water to cover the specimens of first level. The reactor was pressurized using 99.9% pure CO₂, supplied by Air Products. Two different reaction media were thus created, CO₂-saturated water with (HSC) on first level and wet supercritical CO₂ (WSC) on second level. The CO₂ solubility depends on pressure and temperature. At 15 MPa and 90 °C the CO₂ solubility limit in water is 1.02 mol kg⁻¹ and the pH of CO₂-saturated solution is 3.2, and the amount of H₂O in the CO₂-rich phase is relatively small (0.012 mol kg⁻¹), as estimated by the thermodynamic model of Duan and Sun [47].

The evolution of the cement paste degradation process was investigated after 7, 21, and 56 d of exposure to CO₂ environments. All tests were performed under static confinement conditions with no CO₂ reinjection or fluid renewal.

2.4. Evaluation of CO₂ degradation process

The effects of the degradation process on the cement paste properties with and without OMMT nanoclay were evaluated by measuring the depth of the chemically altered layer and analyzing the microstructure changes by scanning electron microscopy (SEM), X-ray microtomography, and X-ray diffraction (XRD). Additionally, the mechanical

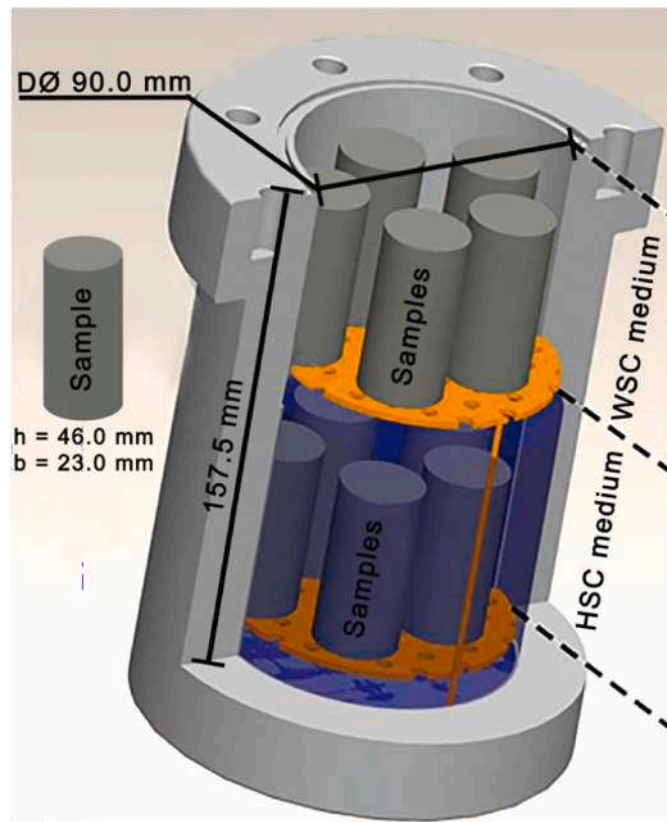


Fig. 3. Experimental arrangement for cement paste degradation tests in CO₂-saturated water (HSC) and wet supercritical CO₂ (WSC).

properties were determined by Vickers microhardness measurements and uniaxial compressive strength tests.

The depth of the chemically altered layer was measured using the Image J software. For each sample, twenty measurements were made along the cross section and the results are presented as an average. Statistical analysis using the bicaudal paired *t*-test (or Student's *t*-test) was applied to confirm if there is a significant difference between the mean and standard deviation of chemically altered layer thicknesses of two groups of samples (with and without OMMT). The null hypothesis is that the average is equal between the two groups, and the alternative hypothesis is that the average is different. If the *p*-value (probability to err by rejecting the null hypothesis) is less than 5% ($p < 0.05$), the null hypothesis was rejected, and there is a significant difference between the averages.

The SEM analyses were performed in a field-emission scanning microscope (Inspect F50 model, FEI). For examination, the samples were cut using a precision diamond saw, ground using silicon carbide sandpaper down to the size of a 1200 mesh, and then mechanically polished with 0.25 μm diamond paste. The samples were covered with a thin conductive gold film.

X-ray powder diffraction was used to identify the main crystalline phases of the cement paste with and without the addition of OMMT, as well as the products consumed and formed in the degradation process in the presence of CO₂. For comparison purposes, X-ray powder diffraction analyses were performed using samples that were extracted from cement specimens exposed to CO₂ environments and unreacted samples. The powder was obtained by crushing and grinding each sample using mortar and pestle. In case of CO₂-reacted specimens, the samples were taken from the chemically modified layer. Analyses were conducted on a Bruker D8 Advance diffractometer, with K α radiation in a copper tube operating with a 40 kV voltage and 30 mA current. The peaks identification was done by using the International Centre for Diffraction Data

(ICDD) database.

3D X-ray computed microtomography was also used to probe the changes in cement density due to CO₂ attack after reaction with CO₂. The equipment used was a SkyScan 1173 X-ray computed microtomograph, operating at 130 kV and 61 μA , yielding a spatial resolution of 7.88 μm . Bruker CTVOX software was used to obtain the images.

The Vickers microhardness test was used to evaluate the hardness changes caused by the carbonation process. The microhardness was measured by applying a load of 100 g for 15 s, and twenty hardness measurements were performed across the chemically altered layer in direction to the core with a step of about 100 μm . The Vickers tests were conducted using a Shimadzu durometer (HMV-2T model) according to ASTM E384-17 standard. The compressive strength tests were performed following the recommendations of ASTM C39/C39M – 18 standard, using a universal testing machine (EMIC, PC200I model) and applying a deformation speed of 0.1 mm/min. The tests were carried out in triplicate for each cementitious paste, and for comparison purpose unreacted samples and CO₂-reacted specimens of same age were tested. For that, the unreacted samples were kept immersed in water since casted for the same period as the specimens in the reactor.

3. Results and discussion

3.1. Properties of cementitious pastes

Results of mini-slump tests performed on distinct fresh cementitious pastes are shown in Fig. 4. Compared to standard cement paste (0% OMMT), the addition of OMMT nanoclay reduces the average spreading diameter of the slurries, leading to a decrease of 13.3%, 16.6%, and 31.4% for 0.5%, 1%, and 2% OMMT contents, respectively. It is well known that the slurry workability is influenced by friction between particles, the particle morphology, and the particle size distribution. The reduction in workability observed by the addition of OMMT nanoclay is probably for the reason that the particles agglutinate the hydrated products, owing to the larger specific area surface at the nanometric scale. Consequently, more water is required to reach an adequate workability.

Fig. 5 shows the specific mass of hardened cementitious pastes with and without OMMT. The addition of nanoclay increases the specific mass of hardened cementitious pastes, but as the OMMT amount increases its effect on matrix densification is less pronounced. The changes in the specific mass of cementitious pastes with 0.5%, 1%, and 2% of OMMT were 13%, 5%, and 2.5%, respectively. This reduction of the specific mass with increasing amount of OMMT can be related to agglomerating, resulting from the difficulty of particles to disperse, as also observed by other authors [14,32–37]. SEM images illustrating

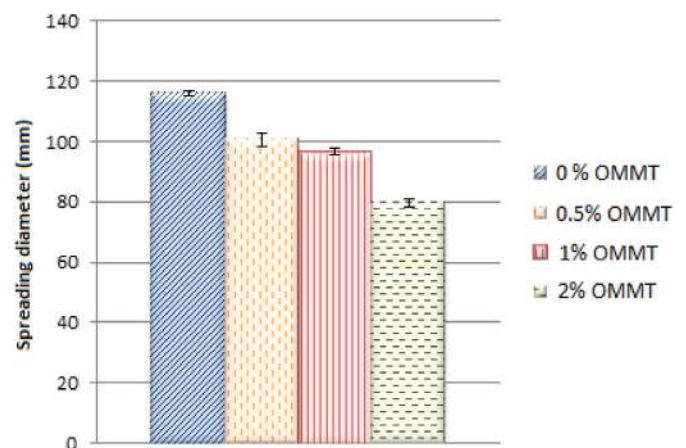


Fig. 4. Results of mini-slump tests performed on fresh cement pastes with and without OMMT nanoclay.

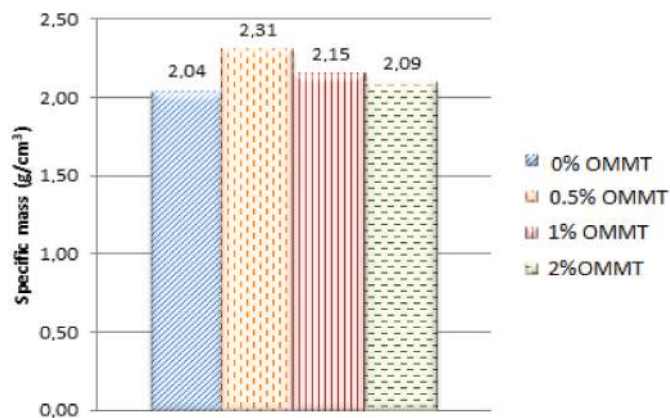


Fig. 5. Specific mass of cement pastes with and without OMMT nanoclay obtained by nitrogen adsorption pycnometry.

OMMT agglomerating in cement paste are shown in Fig. 6.

Fig. 7 shows the compressive strength of cementitious pastes with different amounts of OMMT nanoclay. Notably, the addition of 0.5% of OMMT nanoclay promotes a 24.4% increase in compressive strength. However, the compressive strength decreases with increasing amount of OMMT nanoclay. In general, this property is correlated to specific mass which similarly decreased with increasing of OMMT quantity. Nevertheless, for 2% OMMT addition the specific mass is higher than 0% OMMT but the compressive strength is lower, which could be related to particle agglomeration, as evidenced in Fig. 6.

3.2. Chemical degradation

Fig. 8 shows cross-sectional images of specimens following exposure to HSC and WSC for different periods, and Fig. 9 presents the thicknesses of the chemically modified layer following the carbonation process. The degradation of cement in the presence of CO₂ forms different fronts that are confirmed by the images (Fig. 8). These three zones can be classified from the innermost part to the interface of the CO₂-saturated media: the portlandite depleted zone; the calcium carbonate precipitation zone, and the silica gel zone, where the degradation occurs owing to calcium leaching and CSH decalcification.

Fig. 9 shows the thicknesses of the chemically modified layers for cement pastes with and without OMMT in both reacting media, HSC and WSC. The cement pastes with 0.5% OMMT reacting for 7 d exhibited a significant decreasing in the average thickness of chemically modified layers relative to standard paste (0% OMMT) on *t*-test (*p* < 0.05), corresponding to a reduction in thickness of 28.6% and 27.4% for HS and WSC, respectively. Nevertheless, it is observed that by adding more OMMT nanoclay, the chemically altered layer increases displaying a

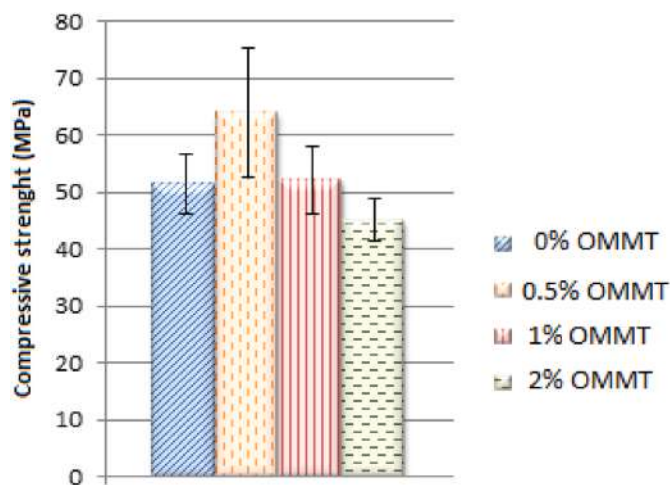


Fig. 7. Compressive strength of cement pastes with and without OMMT nanoclay with 7 days age.

significant difference in relation to standard paste in both medium. This was also observed by Chang et al. [40], who reported that cement properties were only enhanced by adding nanoparticles to less than 1%. The pozzolanic character of OMMT nanoclay induces the formation of more CSH because of the consumption of calcium hydroxide by pozzolanic reactions. The alkaline reserve of the matrix and pore solution is thus reduced, which may facilitate the advance of the carbonation front [48]. HSC medium was the more reactive medium for all pastes for up to 21 d of exposure, whereas WSC medium was more aggressive over 56 d (Fig. 8c).

The computed microtomography images (Fig. 10) evidence the density changes due to chemical reactions with CO₂, where bright orange represents a high density. The sample periphery displays a relatively porous region (the bicarbonate zone), followed by the denser carbonation fronts (paleofronts), then a transition zone between the unaltered nucleus and the porous chemically altered zones (portlandite-depleted zone), and finally the unaltered core. The SEM images (Fig. 11) confirm the computer microtomography results showing the advance of the carbonation fronts. Notably, the carbonation mechanism does not change in the presence of OMMT.

The carbonation process in cement pastes is governed by diffusion and can be modeled as a linear function of the square root of time, according to Fick's second law [18,49,50]. According to Kutchuko et al. [18] and Huet et al. [49], the degradation process tends to deviate from this linear behavior owing to pore clogging by calcium carbonate as the carbonation time increases. Thus, the advance of the degradation front tends to be fast in the first days. However, as calcium carbonate

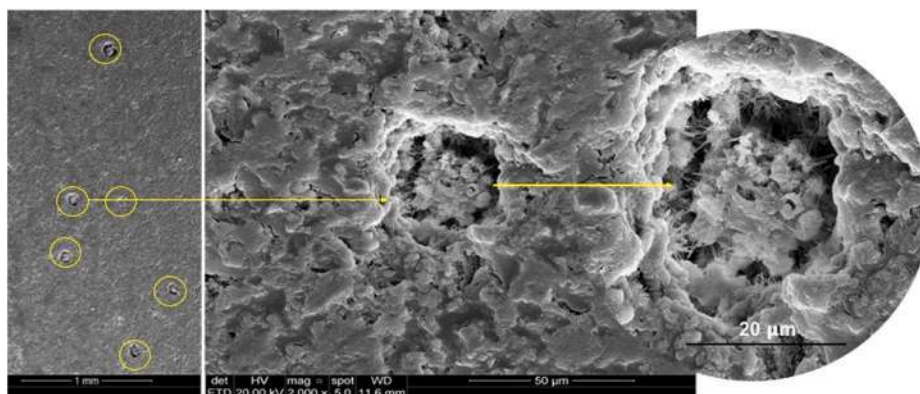


Fig. 6. SEM images showing OMMT nanoclay agglomerating in cement paste with 2% OMMT.

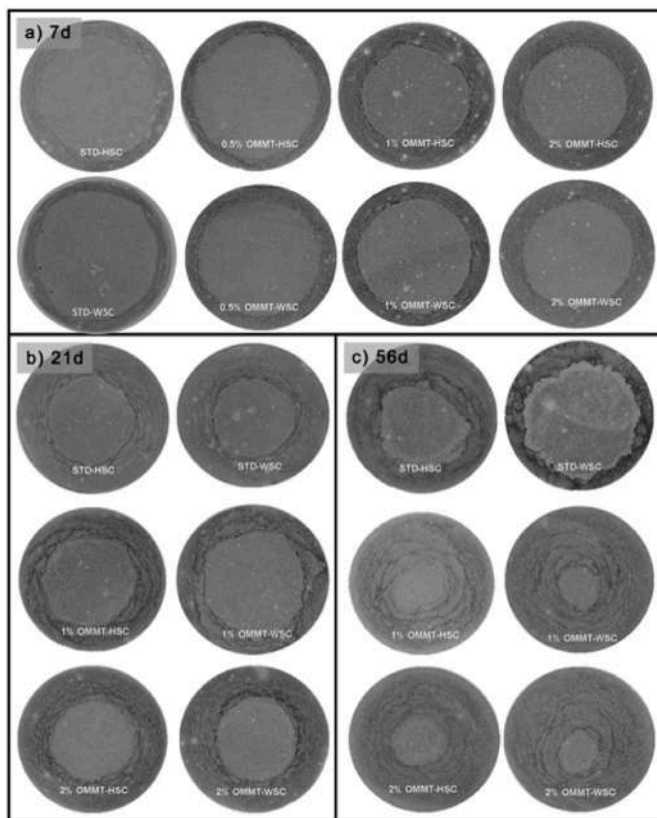


Fig. 8. Cross sections of the cement paste specimens with and without OMMT after exposure to CO₂-rich media for (a) 7 (b) 21 and (c) 56 d.

precipitates in the pores, the permeability decreases, which slows down the carbonation front. A linear function of thickness with square root of time was observed, indicating that the cement paste carbonation process under conditions tested is governed by diffusion. Thus, the diffusion coefficient was calculated by approximating the solution of Fick's second law using a constant concentration boundary condition [18,50], and the results are presented in Table 2. The diffusion coefficient values are in agreement with Barlet-Gouédard et al. [50], who obtained $1.34 \times 10^{-11} \text{ m}^2 \text{ s}^{-1}$. The diffusion coefficient does not exhibit significant difference as verified on *t*-test ($p < 0.05$), either between the media or in the presence or absence of OMMT. The exception was 2% OMMT cement paste, in which the diffusion coefficient was significantly higher than 0% OMMT possibly due to the effects of particle agglomeration.

The diffractogram for the unreacted standard pastes (Fig. 12a and b) indicates the majority presence of the main cement hydrated components, calcium hydroxide (P-portlandite) and calcium silicate hydrate (CSH), indicating the curing efficacy. The X-ray diffraction pattern of the chemically altered layer (Fig. 12c–g) of degraded cement pastes

evidences the presence of calcium carbonate in distinct polymorphic forms, orthorhombic aragonite (A) and rhombohedral calcite (C). The large amount of calcium carbonate is related to the carbonation process, in which hydrated products, calcium hydroxide, and hydrated calcium silicate are consumed by the acid attack. The diffractograms of the degraded layers in the presence of OMMT (Fig. 12b) also display the same components (calcite and aragonite) observed in the diffractogram of the standard paste layer, indicating that the carbonation mechanism occurred in a similar manner. Notably, in the diffractograms from the tests performed over 7 d, the presence of calcium hydroxide is still verified, suggesting that its depletion occurs with longer periods of exposure to CO₂.

3.3. Mechanical properties

Fig. 13a display the results of the Vickers microhardness tests performed on the sample core and the chemically altered layer for HSC medium and Fig. 13b for WSC medium. Microhardness measurements provide important information on the carbonation process since, in the zones where calcium carbonate precipitates, the density increases owing to cement pores filling with carbonate. For both media (HSC and WSC) and for all paste systems (with and without OMMT nanoclay), an increase in the hardness of the chemically altered layer is observed relative to the sample core, as also observed by Kutchko et al. [17]. However, the hardness values do not differ significantly between HSC and WSC. Additionally, a comparison of the hardness of different cement systems reveals similar cement-core hardnesses across all systems, regardless of the presence or absence of OMMT.

However, a comparison of the changes in hardness between the core and chemically altered layer reveals a distinct behavior in the presence of OMMT. Considering only standard paste for all ages and media, the average cement-core hardness is $76.1 \pm 4.4 \text{ HV}/0.1$, whereas the chemically modified layer has an average hardness of $173.3 \pm 5.4 \text{ HV}/0.1$, i.e., a 2.3-fold difference related to the carbonation process. However, all the paste systems containing OMMT nanoclay display an inferior average hardness of the chemically altered layer (approximately 25% lower) relative to standard pastes, and a greater standard deviation. The large standard deviation is probably due to the presence of various degradation fronts with different hardnesses (*paleofronts*), as observed in the SEM images of Fig. 11. The addition of OMMT nanoclay to cement paste affects the microhardness. This could be because the OMMT pozzolanic effect increases the amount of CSH, which tends to make the cement paste less porous, thereby restricting CaCO₃ precipitation in the cement pores. As the carbonated-layer hardness increases, the cementitious material becomes increasingly fragile because the carbonated layer forms an interface with a porous portlandite depleted zone, resulting in impaired mechanical properties under mechanical stress. From this point of view, the addition of OMMT nanoclay can be beneficial for long-term cement integrity in CO₂ rich-environments.

Fig. 14 shows the compressive strength results for all the cement systems before and after exposure to HSC and WSC media over 7 d. For relatively short exposure periods to CO₂ environments (7 d), no

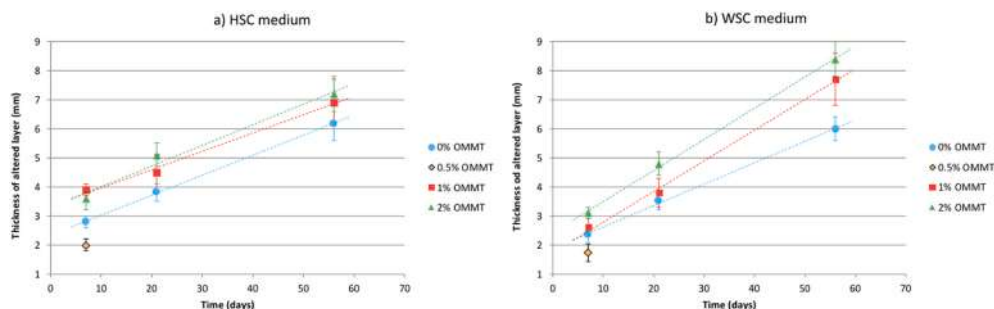


Fig. 9. Thicknesses of the chemically modified layer for different exposure times to CO₂-rich environments.

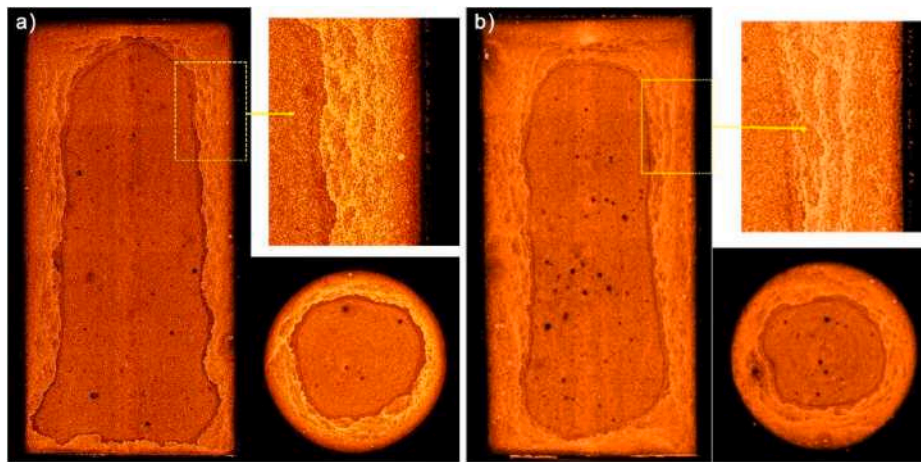


Fig. 10. X-ray computed microtomography images after exposure to CO₂ for (a) standard cement paste (0%OMMT) and (b) cement paste with 1% added OMMT nanoclay.

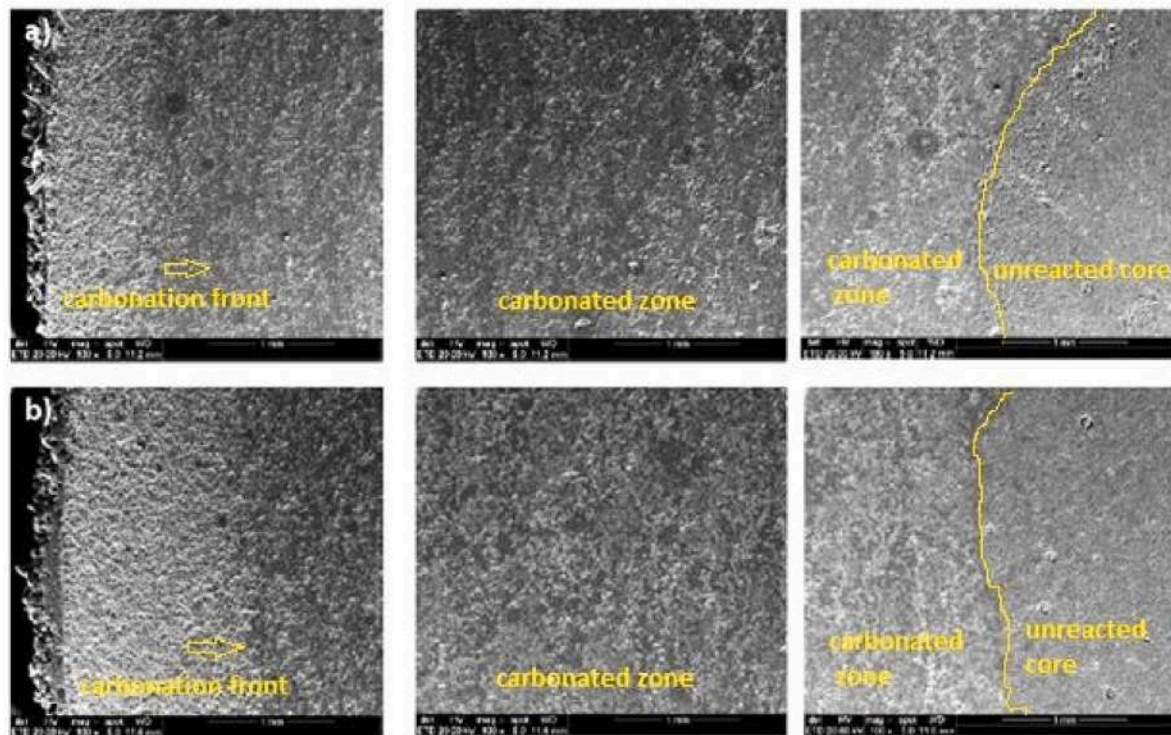


Fig. 11. SEM images of the sample cross-sections exhibiting the advance of the carbonation fronts in the case of (a) 1% of OMMT nanoclay after 21 d and (b) 2% of OMMT nanoclay after 56 d.

Table 2
Diffusion coefficient (m² s⁻¹) for cement systems.

Medium	0% OMMT (Standard paste)	1% OMMT	2% OMMT
HSC	$1.12 \pm 0.16 \times 10^{-11}$	$1.17 \pm 0.28 \times 10^{-11}$	$1.36 \pm 0.20 \times 10^{-11}$
WSC	$1.05 \pm 0.16 \times 10^{-11}$	$1.17 \pm 0.29 \times 10^{-11}$	$1.19 \pm 0.48 \times 10^{-11}$

significant losses in the compressive strength were observed regardless of the presence or absence of OMMT. In some cases, a slight increase in compressive strength was noted, possibly because of the dominance of carbonation over bicarbonation.

Compressive strength test results, obtained before and after exposure to CO₂-rich environments for different cement systems over time, are presented in Fig. 15. An increase in compressive strength over time is observed for all unreacted cement systems, since the cement pastes continued to undergo a slow hydration. The most significant loss in compressive strength (25.6% reduction) was observed for standard paste after 56 d of exposure to WSC medium. In the presence of OMMT nanoclay, the compressive strength decreased by only 13.6% and 8.8% for 1% OMMT in HSC and WSC media, respectively; and by 5.9% for 2% OMMT in WSC medium after 56 d of exposure. This latter result is not very significant, considering the standard deviation. For specimens reacted in HSC medium, no important changes in resistance were observed, but the large standard deviations reflect the heterogeneity of the CO₂-reacted specimens. After 56 d, the unaltered nucleus in the

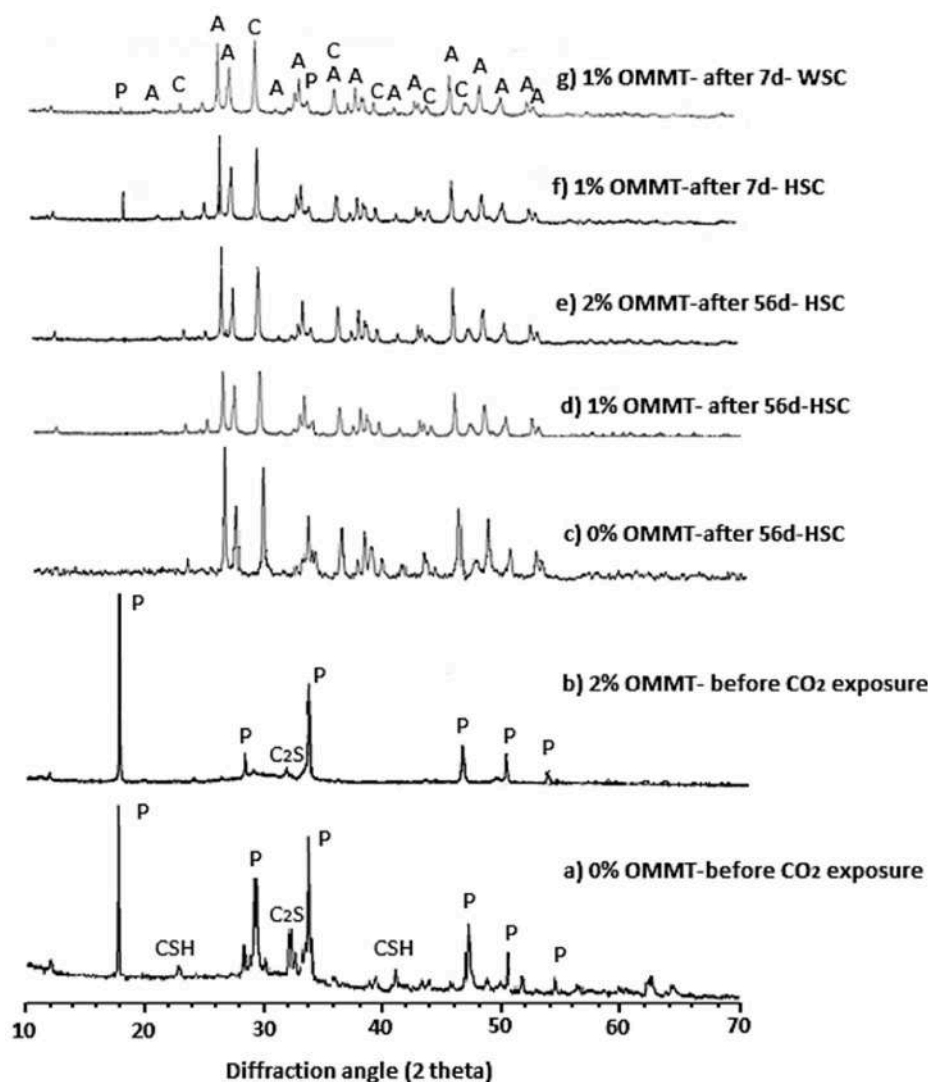


Fig. 12. X-ray diffraction patterns of cementitious pastes before and after exposure to a CO₂ environment. P= Portlandite; CSH= Calcium Silicate Hydrate, C₂S = Dicalcium Silicate = A = Aragonite, C= Calcite.

samples has a diameter of approximately 10 mm, covered by a dense layer consisting predominantly of CaCO₃, as shown in Fig. 8c. These results indicate that the compressive strength tends to be considerably affected after long exposures to CO₂.

In summary, the results suggest that the inclusion of OMMT nanoclay in oil-well cement is likely to preserve the compressive strength of the cement in CO₂-rich environments. This effect is possibly due to pozzolanic reactions promoted by the OMMT nanoclay that reduces the portlandite content, allowing the formation of a secondary chain of CSH. This in turn promotes a denser cementitious matrix, as confirmed by the specific mass analyses. However, the cement blends with higher OMMT content (2%) displayed a compressive resistance that was slightly lower than the standard paste, possibly because of OMMT nanoclay agglomeration. These results evidence the importance to developing a more efficient mixture process that allows to reach a more homogeneous OMMT-cement based composite.

The detachment and rupture of the degraded layer during the compressive strength tests were verified, as illustrated in Fig. 16a for standard paste specimens. This behavior could be related to the large difference between the hardnesses of the core and chemically degraded layer, which are separated by a highly porous zone (portlandite-depleted zone) with a low mechanical strength. The occurrence of fractures and

the separation of the chemically altered layer during the compressive strength test observed in the standard paste specimens indicates the possibility of a similar behavior in oil-wells, since the cement annulus is subjected to mechanical stresses associated with pressure variations during periods of CO₂ injection or during contractions and expansions due to thermal gradients. In addition, such fractures can produce preferential pathways for CO₂ migration, resulting in the exposure of the entire cement-paste core to the acid medium and hence accelerating the degradation of the cement paste. However, this fracture mechanism was not observed in the specimens with OMMT nanoclay, as shown in Fig. 16b. This suggests that, in the presence of OMMT, the change in hardness between the carbonated layer and the portlandite zone is smoother or the dissolution of portlandite is not as pronounced and porous as that of the standard paste, possibly associated to lower portlandite amount present in cement hydrated paste promoted by OMMT pozzolanic effect. The cement paste may thus resist longer periods of acid attack in the presence of mechanical stresses. However, further studies are needed to better understand the effects of nanoclay on the process of hydration, carbonation for longer periods of exposure to CO₂ and failure mechanisms of oil-well cement paste.

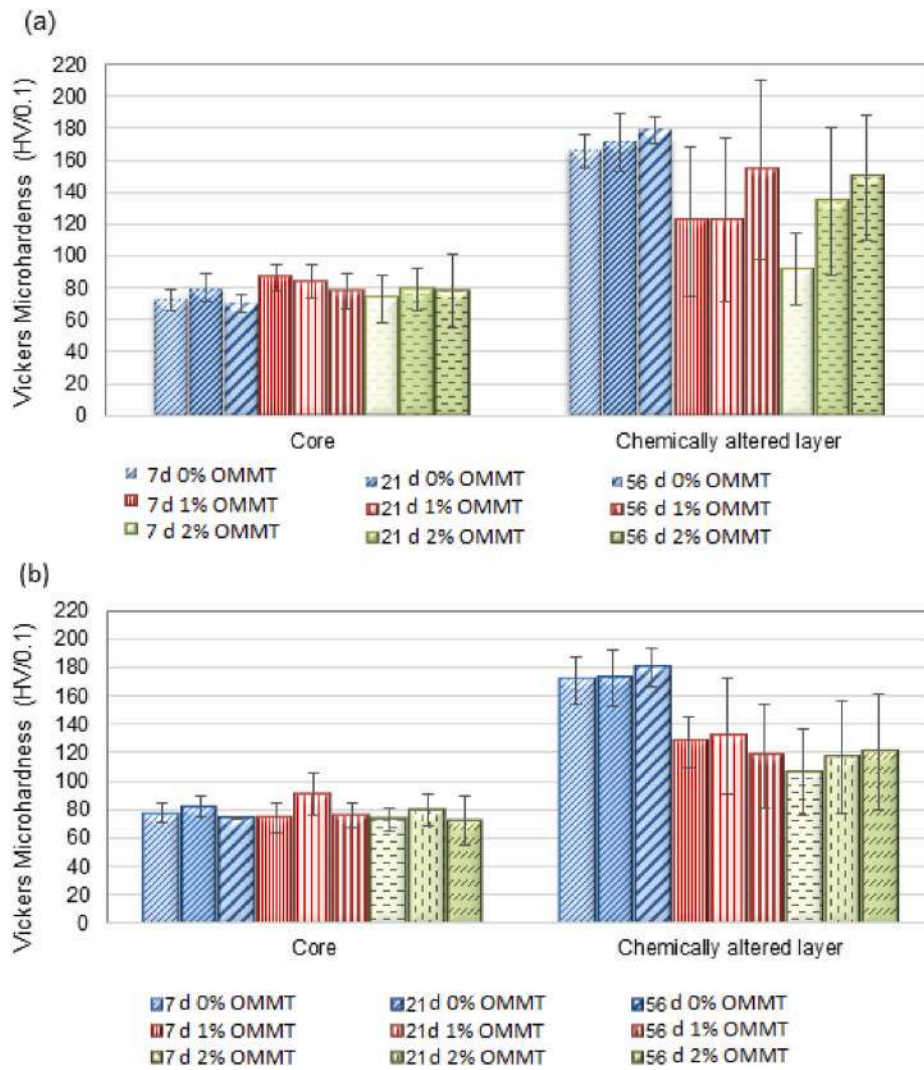


Fig. 13. Vickers microhardness of the core and chemically altered layer regions after exposure of the cement samples with and without OMMT nanoclay. a) HSC medium and (b) WSC medium.

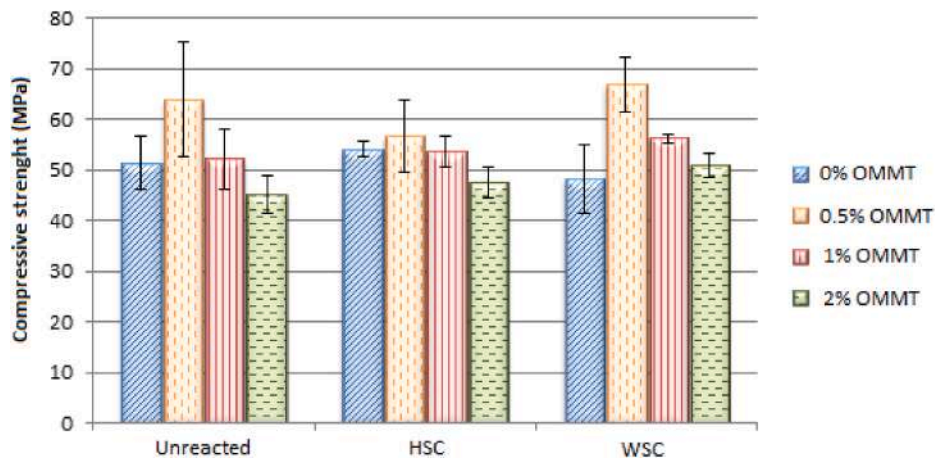


Fig. 14. Compressive strength of cement pastes with and without OMMT nanoclay before and after exposure to HSC or WSC medium for 7 d.

4. Conclusions

From the research reported in this paper about the effect of adding organo-modified montmorillonite nanoclay on the performance of oil-

well cement paste in CO₂-rich environments the following conclusions can be drawn:

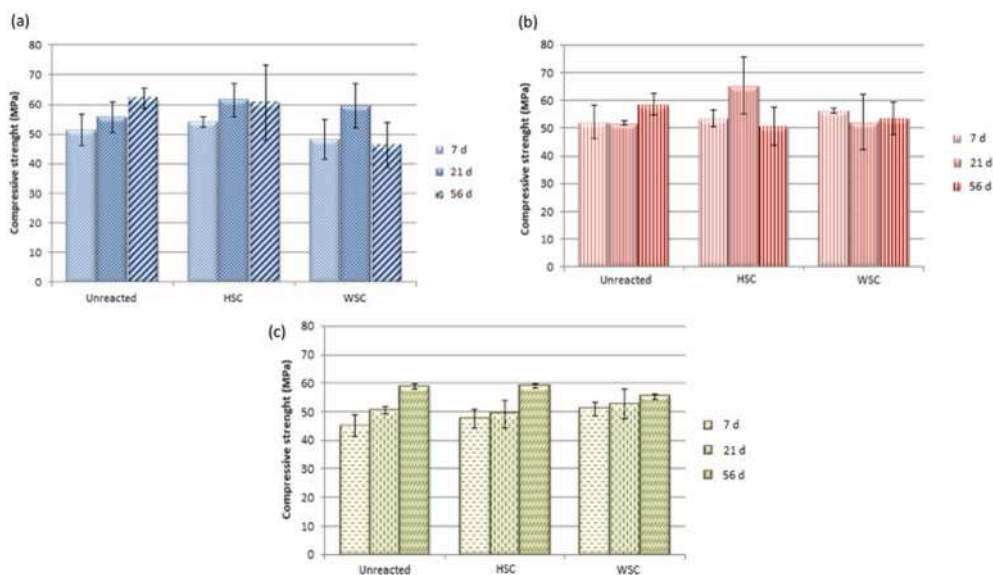


Fig. 15. Compressive strength of OMMT cement systems before and after exposure to HSC or WSC medium for different periods. (a) standard cement paste (0% OMMT). (b) 1% OMMT. (c) 2% OMMT.

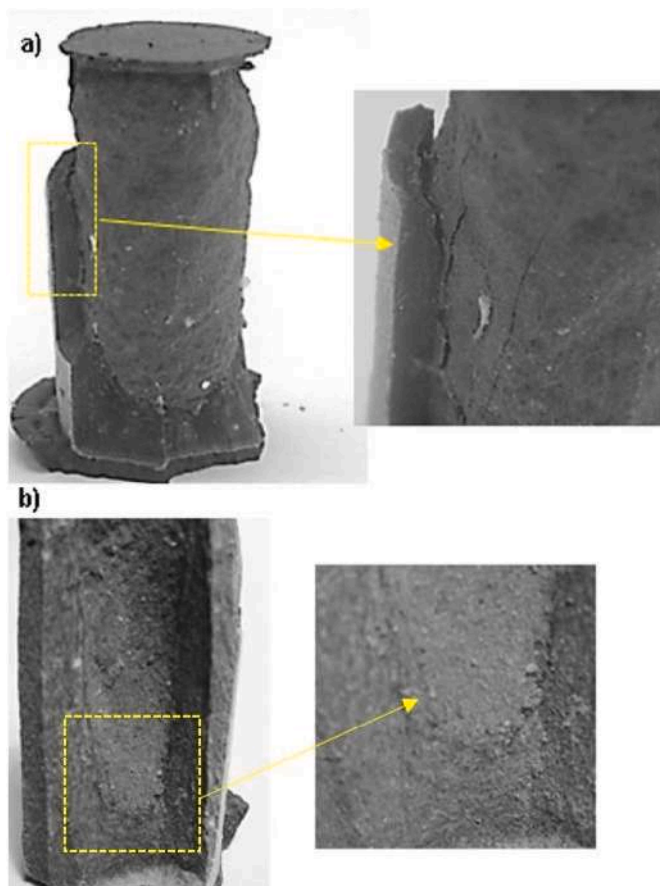


Fig. 16. Image of the fracture in specimens during compressive strength tests after 21 d in WSC medium for (a) standard cement paste (0%OMMT) and (b) cement paste with 2% OMMT.

- The addition of OMMT nanoclay reduces the workability of cement slurries and promotes a slight increase in specific mass;
- The cement containing OMMT nanoclay exhibited the same reaction mechanism reported in the literature for regular oil-well cement

class G in CO₂-rich environments, involving the formation of three zones: a highly porous portlandite-depleted zone, a carbonated zone composed of calcium carbonate in polymorphic forms of aragonite and calcite of high density, and the bicarbonated zone. However, microhardness measurements showed that the carbonated zone in standard paste is harder than in cement systems containing OMMT nanoclay;

- The addition of 1% and 2% of OMMT nanoclay in cement paste promoted an increase in the chemically altered layer due to carbonation in presence of CO₂, but for 0.5% OMMT it decreased. This indicates that, for some suitable particle content, resistance to chemical attack in the presence of CO₂ can be enhanced, as reported previously in the literature when adding nanoparticles to cement;
- The addition of OMMT nanoclay maintains the compressive strength when the cement is exposed to a CO₂-rich environment, possibly because of the increase in the pozzolanic reactions promoted by the nanoclay;
- Specimens with nanoclay tended not to display a detachment of the chemically altered layer during the compressive test. This suggests that the presence of nanoparticles does not promote the formation of a pronounced portlandite dissolution region, as is apparent in their absence, indicating that they can maintain structural integrity for longer periods, even under acid attack and mechanical stress.

Declaration of competing interest

The authors declare that they have no known competing financial interests or personal relationships that could have appeared to influence the work reported in this paper.

Acknowledgements

The authors acknowledge support from the CNPq (The Brazilian Research Council) and the Institute of Petroleum and Natural Resources. This study was financed in part by the Coordenação de Aperfeiçoamento de Pessoal de Nível Superior – Brasil (CAPES) – Finance Code 001.

References

- [1] IPCC, in: O. Edenhofer, R. Pichs-Madruga, Y. Sokona, E. Farahani, S. Kadner, K. Seyboth, A. Adler, I. Baum, S. Brunner, P. Eickemeier, B. Kriemann, J. Savolainen, S. Schlömer, C. von Stechow, T. Zwickel, J.C. Minx (Eds.), *Climate*

- Change 2014: Mitigation of Climate Change. Contribution of Working Group III to the Fifth Assessment Report of the Intergovernmental Panel on Climate Change, Cambridge University Press, Cambridge, United Kingdom and New York, NY, USA, 2014.
- [2] V. Arora, R.K. Saran, R. Kumar, S. Yadav, Separation and sequestration of CO₂ in geological formations, *Mater. Sci. Eng. Technol.* 2 (2019) 647–656.
 - [3] S. Bachu, Sequestration of CO₂ in geological media: criteria and approach for site selection in response to climate change, *Energy Convers. Manag.* 41 (2000) 953–970.
 - [4] B. Cailly, P. Le Thiez, P. Egermann, A. Audibert, S. Vidal-Gilbert, X. Longaygue, Geological storage of CO₂: a state-of-the-art of injection Processes and Technologies, *Oil Gas Sci. Technol.* 60 (2005) 517–525.
 - [5] M. Davarazar, D. Jahanianfard, Y. Sheikhejad, B. Nemati, T.M. Aminabhavi, Underground carbon dioxide sequestration for climate change mitigation—A scientometric study, *J. CO₂ Util.* 33 (2019) 179–188.
 - [6] A. Raza, R. Gholami, R. Rezaee, V. Rasouli, M. Rabiei, Significant aspects of carbon capture and storage – a review, *Petroleum* 5 (2018) 335–340.
 - [7] S. Størset, G. Tangen, D. Berstad, P. Eliasson, M. Torsæter, Profiting from CCS innovations: a study to measure potential value creation from CCS research and development, *Int. J. Greenh. Gas Control* 83 (2019) 208–215.
 - [8] T. Wilberforce, A. Baroutaji, B. Souda, A.H. Al-Alami, A.G. Olabi, Outlook of carbon capture technology and challenges, *Sci. Total Environ.* 657 (2019) 56–72.
 - [9] M. Bentham, G. Kirby, CO₂ storage in saline aquifers, *Oil Gas Sci. Technol.* 60 (2005) 559–567.
 - [10] J.Q. Shi, S. Durucan, CO₂ Storage in deep unminable coal seams, *Oil Gas Sci. Technol.* 60 (2005) 547–558.
 - [11] T. Wildenborg, A. Lokhorst, Introduction on CO₂ geological storage. Classification of storage options, *Oil Gas Sci. Technol.* 60 (2005) 513–515.
 - [12] F. Gozalpour, S.R. Ren, B. Tohidi, CO₂ EOR and storage in oil reservoirs, *Oil Gas Sci. Technol.* 60 (2005) 537–546.
 - [13] J. Iyer, J. Chen, S.A. Carroll, Impact of chemical and mechanical processes on leakage from damaged wells in CO₂ storage sites, *Environ. Sci. Technol.* 54 (2020) 1196–1203.
 - [14] K. Abid, R. Gholami, P. Choate, B.H. Nagaratnam, A review on cement degradation under CO₂-rich environment of sequestration projects, *J. Nat. Gas Sci. Eng.* 27 (2015) 1149–1157.
 - [15] V. Barlet-Gouédard, G. Rimmelé, B. Goffé, O. Porcherie, Well technologies for CO₂ geological storage: CO₂-resistant cement, *Oil Gas Sci. Technol.* 62 (2007) 325–334.
 - [16] J.W. Carey, M. Wigand, S.J. Chipera, G. WoldeGabriel, R. Pawar, P.C. Lichtner, S. C. Wehner, M.A. Raines, G.D. Guthrie Jr., Analysis and performance of oil well cement with 30 years of CO₂ exposure from the SACROC Unit, West Texas, USA, *Int. J. Greenh. Gas Control* 1 (2007) 75–85.
 - [17] B.G. Kutchko, B.R. Strazisar, G.A. Lowry, N. Thaulow, Degradation of well cement by CO₂ under geologic sequestration conditions, *Environ. Sci. Technol.* 41 (2007) 4787–4792.
 - [18] B.G. Kutchko, B.R. Strazisar, G.A. Lowry, D.A. Dzombak, N. Thaulow, Rate of CO₂ attack on hydrated class H well cement under geologic sequestration conditions, *Environ. Sci. Technol.* 42 (2008) 6237–6242.
 - [19] A. Duguid, J.W. Carey, R. Butsch, Well integrity assessment of a 68 years old well at a CO₂ injection project, *Energy Proc.* 63 (2014) 5691–5706.
 - [20] Q. Li, W.M. Lim, K.M. Flores, K. Kranjc, Y. Jun, Chemical reactions of Portland cement with aqueous CO₂ and their impacts on cement's mechanical properties under geologic CO₂ sequestration conditions, *Environ. Sci. Technol.* 49 (2015) 6335–6343.
 - [21] M. Zhang, S. Talman, Experimental study of well cement carbonation under geological storage conditions, *Energy Proc.* 63 (2014) 5813–5821.
 - [22] A. Shahval, R. Azin, A. Zamani, Cement design for underground gas storage well completion, *J. Nat. Gas Sci. Eng.* 18 (2014) 149–154.
 - [23] A. Brandl, J. Cutler, A. Seholm, M. Sansil, G. Braun, Cementing solutions for corrosive well environments, *Society of Petroleum Engineers - SPE Drilling & Completion* 26 (2011) 208–219.
 - [24] A.K. Santra, B.R. Reddy, F. Liang, R. Fitzgerald, Reaction of CO₂ with Portland cement at downhole conditions and the role of pozzolanic supplements. *Society of Petroleum Engineers*, in: SPE International Symposium on Oilfield Chemistry. The Woodlands, Texas, April 2009.
 - [25] M. Bai, J. Sun, K. Song, L. Li, Z. Qiao, Well completion and integrity evaluation for CO₂ injection wells, *Renew. Sustain. Energy Rev.* 45 (2015) 556–564.
 - [26] M. Bagheri, S.M. Shariatipour, E. Ganjian, A review of oil well cement alteration in CO₂-rich environments, *Construct. Build. Mater.* 186 (2018) 946–968.
 - [27] R.B. Ledesma, N.F. Lopes, K.G. Bacca, M.K. Moraes, G.S. Batista, M.R. Pires, E. M. Costa, Zeolite and fly ash in the composition of oil well cement: evaluation of degradation by CO₂ under geological storage condition, *J. Petrol. Sci. Eng.* 185 (2020) 106656.
 - [28] M.J. Hanus, A.T. Harris, Nanotechnology innovations for the construction industry, *Prog. Mater. Sci.* 58 (2013) 1056–1102.
 - [29] S.C. Paul, A.S. van Rooyen, G.P.A.G. van Zijl, L.F. Petrik, Properties of cement-based composites using nanoparticles: a comprehensive review, *Construct. Build. Mater.* 189 (2018) 1019–1034.
 - [30] F. Sanchez, K. Sobolev, Nanotechnology in concrete – a review, *Construct. Build. Mater.* 24 (2010) 2060–2071.
 - [31] J.D. Mangadiao, P. Cao, R.C. Advincula, Smart cements and cement additives for oil and gas operations, *J. Petrol. Sci. Eng.* 129 (2015) 63–76.
 - [32] J. Chen, S.C. Kou, C.S. Poon, Hydration and properties of nano-TiO₂ blended cement composites, *Cement Concr. Compos.* 34 (2012) 642–649.
 - [33] M. Choolaei, A.M. Rashidi, M. Ardjmand, A. Yadegari, The effect of nanosilica on the physical properties of oil well cement, *Mater. Sci. Eng. A* 538 (2012) 288–294.
 - [34] N. Jafariefad, M.R. Geiker, Y. Gong, P. Skalle, J. He, Cement sheath modification using nanomaterials for long-term zonal isolation of oil wells: Review, *J. Petrol. Sci. Eng.* 156 (2017) 662–672.
 - [35] M. Khalil, B.M. Jan, C.W. Tong, M.A. Berawi, Advanced nanomaterials in oil and gas industry: design, application and challenges, *Appl. Energy* 191 (2017) 287–310.
 - [36] S. Ko, C. Huh, Use of nanoparticles for oil production applications, *J. Petrol. Sci. Eng.* 172 (2019) 97–114.
 - [37] P. McElroy, H. Emadi, K. Surowiec, D.J. Casadonte, Mechanical, rheological, and stability performance of simulated in-situ cured oil well cement slurries reinforced with alumina nanofibers, *J. Petrol. Sci. Eng.* 183 (2019) 106415.
 - [38] W.Y. Kuo, J.-S. Huang, C.-H. Lin, Effects of organo-modified montmorillonite on strengths and permeability of cement mortars, *Cement Concr. Res.* 36 (2006) 886–895.
 - [39] P. Hosseini, R. Hosseinpouria, A. Pajum, M.M. Khodavirdi, H. Izadi, A. Vaezi, Effect of nano-particles and aminosilane interaction on the performances of cement-based composites: an experimental study, *Construct. Build. Mater.* 66 (2014) 113–124.
 - [40] T.P. Chang, J.Y. Shih, K.M. Yang, Material properties of Portland cement paste with nano- montmorillonite, *J. Mater. Sci.* 42 (2007) 7478–7487.
 - [41] P. Yu, Z. Whang, P. Lai, P. Zhang, J. Wang, Evaluation of mechanic damping properties of montmorillonite/organo-modified montmorillonite-reinforced cement paste, *Construct. Build. Mater.* 203 (2019) 356–365.
 - [42] M.L. Nehdi, Clay in cement-based materials: critical overview of state-of-the-art, *Construct. Build. Mater.* 51 (2014) 372–382.
 - [43] API 10A, Specification for Cements and Materials for Well Cementing, 2009.
 - [44] D.L. Kantro, Influence of water-reducing admixtures on properties of cement paste-A miniature slump test, *Cem. Concr. Aggregates* 2 (2) (1980) 95–102.
 - [45] X. Pang, W.C. Jimenez, B.J. Iverson, Hydration kinetics modeling of the effect of curing temperature and pressure on the heat evolution of oil well cement, *Cement Concr. Res.* 54 (2013) 69–76.
 - [46] B. van der Meer, Carbon dioxide storage in natural gas reservoirs, *Oil Gas Sci. Technol.* 60 (2005) 527–536.
 - [47] Z. Duan, R. Sun, An improved model calculating CO₂ solubility in pure water and aqueous NaCl solutions from 273 to 533 K and from 0 to 2000 bar, *Chem. Geol.* 193 (2003) 257–271.
 - [48] A. Çolak, Characteristics of pastes from a Portland cement containing different amounts of natural pozzolan, *Cement Concr. Res.* 33 (2003) 585–593.
 - [49] B. Huet, V. Tasoti, I. Khalfallah, A review of Portland cement carbonation mechanisms in CO₂ rich environment, *Energy Proc.* 4 (2011) 5275–5282.
 - [50] V. Barlet-Gouédard, G. Rimmelé, B. Goffé, O. Porcherie, Mitigation Strategies for the Risk of CO₂ Migration through Wellbores, IADC/SPE 98924, Miami, USA, February, 2006.